Constraints on dark energy and its models

Dragan Huterer[1], Eric V. Linder[2] and Jochen Weller[3]
[1] *Department of Physics, The University of Chicago, Chicago, IL 60637-1433*
[2] *E. O. Lawrence Berkeley National Laboratory, Berkeley, CA 94720*
[3] *DAMTP, Centre for Mathematical Sciences, Wilberforce Road, Cambridge, CB3 0WA, U.K.*

I. INTRODUCTION

The two most conspicuous features of dark energy are smooth spatial distribution and large negative pressure. While only vacuum energy is absolutely uniform in its spatial distribution, all the other examples of dark energy only clump on the largest scales at a level that can be neglected for most purposes. In the absence of a compelling theoretical model or framework for dark energy it can be parameterized by its bulk equation of state: $w \equiv \langle p_\phi \rangle / \langle \rho_\phi \rangle$ (e.g., -1 for vacuum energy, or $-N/3$ for topological defect networks of dimensionality N). Since w is in general time-varying (e.g., in dynamical scalar field models), the first step toward solving the dark energy problem is determining $w(t)$.

In this article we discuss constraint of dark energy using type Ia supernova (SNe Ia) data of the quality expected from the proposed SNAP mission.

II. CONSTRAINING THE EQUATION OF STATE PARAMETER

Initially we assume that the dark energy equation of state does not change in time, $w(z) = w = \text{const}$. Not only does this hold for models with truly constant w (vacuum energy, domain walls and cosmic strings, etc.) but some models with time-variable equation of state can have $w(z) \approx \text{const}$ out to $z \sim 2$.

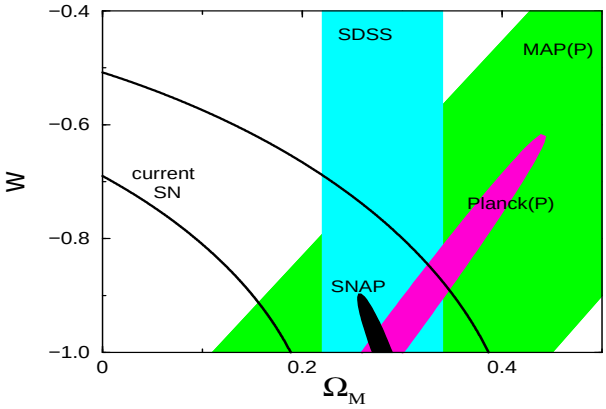

FIG. 1: Projected SNAP constraint compared to those projected for MAP and Planck (with polarization information) and SDSS. Also shown are the present bounds using a total of 54 SNe Ia. All constraints assume a flat Universe with $\Omega_M = 1 - \Omega_\phi = 0.28$ and *constant* equation of state factor with fiducial value $w = -1$. The plot is taken from Ref. [8], and all contours are 68% confidence intervals.

Fig. 1 shows that a supernova program, such as SNAP with ∼2500 supernovae out to $z = 1.7$, will enable very accurate measurement of w: $\sigma_w \approx 0.05$, after marginalization over Ω_M and assuming a flat Universe. This figure also shows constraints anticipated from the Sloan Digital Sky Survey (SDSS) and MAP and Planck satellites (with polarization information).

But the time-variation of w is an important probe of the nature of dark energy. Evolving scalar field models generically exhibit time-variable w, with significant variation out to $z \sim 1$ (e.g. with PNGB scalar field models [2]

and some tracker quintessence models [3, 4]). So these models pose a detectable distinction from the cosmological constant or cosmic defects, and often from each other.

The simplest way to parameterize the evolution of w is by first-order Taylor expansion [5–7]

$$w = w_0 + w_1 z\,. \tag{1}$$

The energy density in the dark component is then given by

$$\rho_\phi(z) = \rho_\phi(z=0)(1+z)^{3(1+w_0-w_1)} e^{3w_1 z}, \tag{2}$$

and the coordinate distance in a flat universe is

$$r(z) = \frac{c}{H_0}\int_0^z \frac{(1+z')^{-3/2}}{\sqrt{\Omega_{\rm m} + \Omega_\phi\,(1+z')^{3(w_0-w_1)}\,e^{3w_1 z'}}}\,dz'\,, \tag{3}$$

which allows us to calculate the magnitude redshift relation for arbitrary combinations of w_0 and w_1.

Using the Fisher matrix formalism, we determine the error ellipses in the w_0-w_1 plane; the constraint to $w(z)$ follows by computing

$$\sigma_{w(z)} = \sqrt{\sigma_{w_0}^2 + \sigma_{w_1}^2\, z^2}. \tag{4}$$

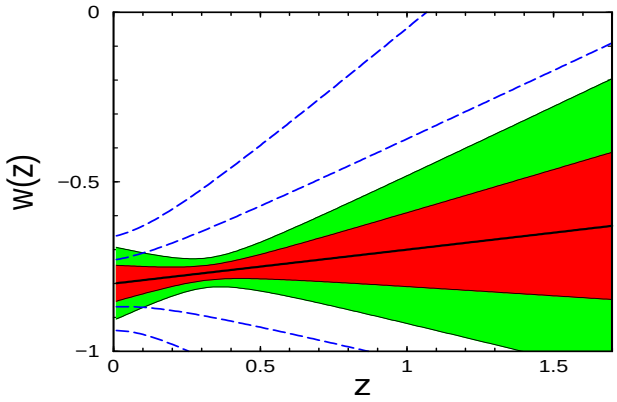

FIG. 2: 68% and 95% c.l. constraints on $w(z)$ using simulated SNAP data, assuming a linear expansion of w in redshift and around a fiducial model $w(z) = -0.8 + 0.1z$. The shaded regions assume a perfectly known Ω_M, while the dashed lines show the effect of assuming a Gaussian uncertainty of 0.05 in Ω_M. The plot is taken from Ref. [8].

Fig. 2 illustrates the constraint to $w(z)$ assuming the SNAP dataset. Cosmological observations have diminishing leverage at both high and low redshift, which is reflected in the narrow "waist" at $z \sim 0.35$ – this is the sweet spot in sensitivity to $w(z)$ (see Ref. [8] for more details).

A more general way to constrain $w(z)$ is to parameterize it by constant values in several redshift bins, since no particular form for $w(z)$ need be assumed. We divide the SNAP redshift range into B bins centered at redshifts z_i with corresponding widths Δz_i and equation of state factors w_i $(i = 1, \ldots, B)$. The energy density of the dark component evolves as (for z in bin j)

$$\rho_\phi(z) = \rho_\phi(z=0)\,\left(\frac{1+z}{1+z_j-\Delta z_j/2}\right)^{3(1+w_j)} \prod_{i=1}^{j-1}\left(\frac{1+z_i+\Delta z_i/2}{1+z_i-\Delta z_i/2}\right)^{3(1+w_i)}. \tag{5}$$

To obtain the constraints using this approach, we again employ the Fisher matrix formalism, treating w_i as the parameters to be determined.

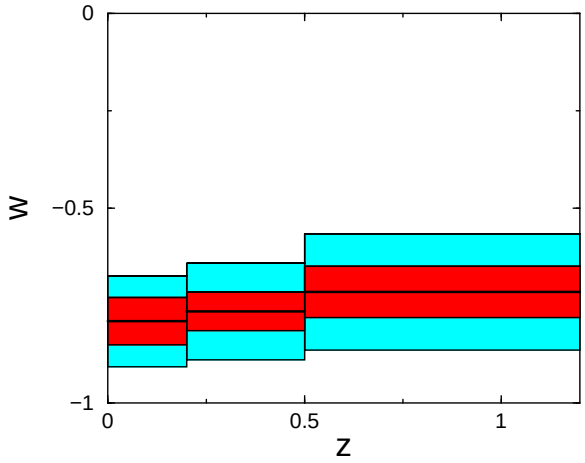

FIG. 3: Here $w(z)$ is parameterized by constant values in redshift bins for the same fiducial model as Fig. 2. The outer region shows 68% cl constraints corresponding to each redshift bin. The inner region shows 68% cl constraints when a Gaussian prior is imposed that penalizes models with a large change in w between two adjacent bins. The plot is taken from Ref. [8].

Fig. 3 shows constraints on $w(z)$ when w is parameterized by values in three redshift bins whose widths are chosen so that the uncertainty in each is about the same. Flatness and precise knowledge of Ω_M were assumed. The constraints are not strong ($\sigma_w \approx 0.12$) in part because the values of w in adjacent bins are uncorrelated. Many models with time-dependent equation of state have $w(z)$ that vary slowly (or not at all) out to $z \sim 1$. Therefore, we also show results when a Gaussian prior is imposed that penalizes models with large change in w between two adjacent bins (the prior is a Gaussian in $w_{i+1} - w_i$ with standard deviation $\sigma = 0.10$). The 1σ constraints improve by more than a factor of two.

III. CONSTRAINING SPECIFIC DARK ENERGY MODELS

In recent years a plethora of scalar field theories to account for the accelerated expansion of the universe have been proposed. One of the earliest suggestions was a scalar field with a pure exponential potential [9]. This potential exhibits an attractor behavior, which obviates the fine-tuning of initial conditions. Unfortunately, in the attractor regime this potential can not explain the observed acceleration today. A powerful extension to this model is the class of so called cosmological tracker solutions [3, 4]. These models also have an attractor behavior, but the energy density in the scalar field dominates eventually over the other contributions, causing the universe to start accelerating. Other models in the literature adapt the features of the pure exponential potential [10] or incorporate a periodic potential [2].

[Exceptions to the complete characterization of the dynamics of dark energy models by their equation of state are non-minimally coupled scalar field cosmologies or scalar tensor gravity theories, which need specification of the coupling function [11]. We do not discuss this class of models any further in this context, but note that it should be possible to encode most of the dynamics of these models in an effective equation of state factor.]

Fig. 4 illustrates the late time redshift evolution $w(z)$ for various dark energy described in [7]. Note that while most of the models shown behave quite differently from a cosmological constant ($w = -1$), some allow solutions mimicking $w = -1$ over a wide redshift range if the parameters are chosen appropriately.

In Fig. 5 we show the magnitude difference Δm relative to a fiducial cosmological constant model with $\Omega_{\rm m} = 0.3$ and $\Omega_\phi = 0.7$. The binned data points are are obtained by simulating mock observations with SNAP specifications and the fiducial cosmology. We recognize that for the *2EXP* model a constant w fit is sufficient, while for the *SUGRA* model we require a linear fit. This plot already gives insight on to what level SNAP will be able to distinguish different cosmological models.

In order to quantify the expected confidence limits on the parameters from supernovae observations with SNAP, we simulated data for some of the models and calculated the likelihood with a χ^2 statistic.

Fig. 6 shows the joint likelihood contours in the $\Omega_{\rm m} - w_0$ plane with a constant w fit. The flanking light shaded contours are the effects due to a drifting systematic error of ± 0.02mag per 1.5 units in redshift. We see that the shift

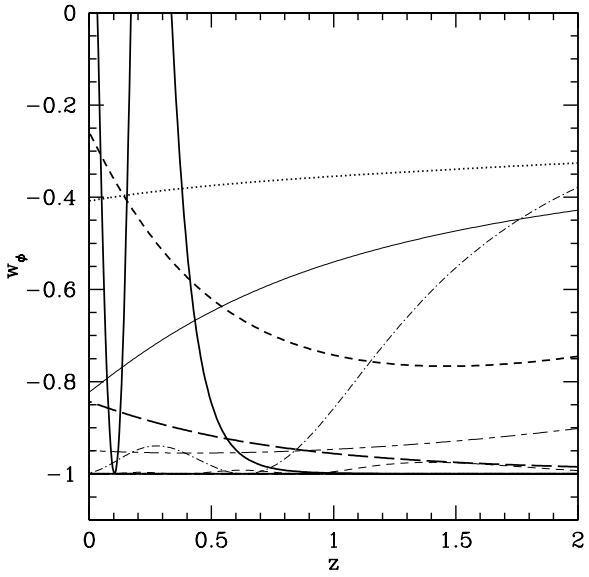

FIG. 4: The redshift evolution of equation of state factor $p_\phi = w\rho_\phi$ for the discussed models. The thin short dash line is the Albrecht & Skordis model [10], the thin dot - short dash line is from the brane inspired potential [10], the thin short dash - long dash line from the potential which involves two exponentials [10], the thick short dashed line from the periodic potential [2], the thick long dashed line from the pure exponential [9], the thick solid line from the Pseudo Nambu-Goldstone Boson potential [2], the thin solid line from the Supergravity inspired potential [4], the thin long dashed line from the exponential tracker solution (underneath $w = -1$) [4], and the thick dotted line from the inverse tracker. The plot is taken from [7].

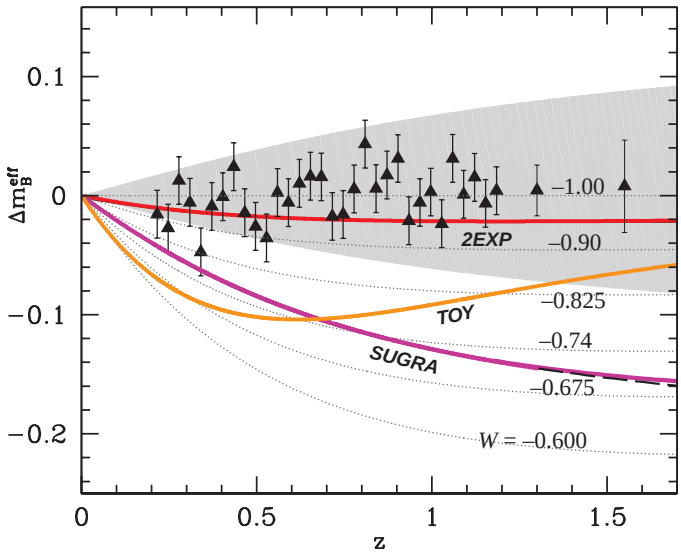

FIG. 5: Simulated binned data, with solid curves from a Supergravity inspired model [3, 4] (with the best $w_0 - w_1$ expansion fit shown as a dashed line, mostly covered by the solid *SUGRA* line), a strongly evolving toy model with $w_0 = -0.6$ and $w_1 = -0.8$ (*TOY*), and a model involving two exponentials [10] (*2EXP*). A range of constant w models is shown as a grid of dotted lines. The shaded region corresponds to cosmological constant models with $0.25 \leq \Omega_m \leq 0.35$. The plot is taken from [6].

due to systematics is roughly one statistical standard deviation in the Ω_m direction, but there are hardly any changes in the w_0 direction. Clearly the data will discriminate among the models shown.

We now analyze the same simulated data using a fitting function that includes w_1. For this analysis (results shown

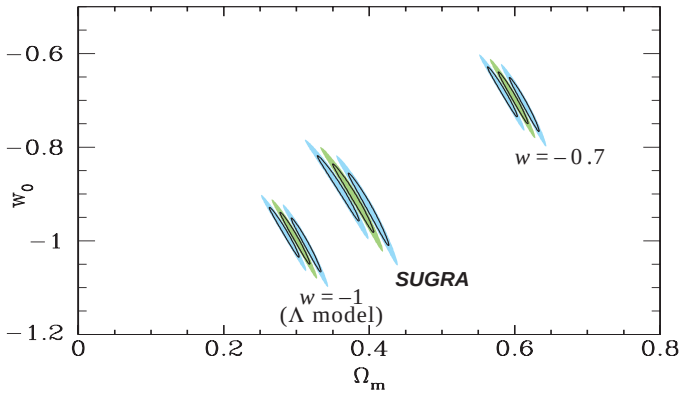

FIG. 6: Separation of dark energy models (labeled as in Fig. 5) in the $\Omega_{\rm m}$–w_0 plane. We show 39.3% ($\Delta\chi^2 = 1$, shown as solid-line contours) and 68% ($\Delta\chi^2 = 2.3$, shown as shaded contours) confidence regions which project on the axes to give marginalized 1σ and 1.5σ errors respectively. The left and right flanking contours for each model show the effects of a drifting systematic error (see text). The $w = -0.7$ model has $\Omega_m = 0.6$. This plot is from [6].

prior σ_{Ω_m}	measurement $\sigma_{\rm mag}$	σ_{w_0}	σ_{w_1}
No Ω_m prior; $w_1 = 0$	0.15	0.06	
0.15	0.15	0.15	0.6
0.05	0.15	0.06	0.2
"	*0.09*	*0.05*	*0.12*
0.04	0.15	0.05	0.16
0 (fixed Ω_m)	0.15	0.03	0.12

TABLE I: Statistical measurement uncertainties on w_0 (i.e., $w_{\rm today}$) and w_1, given supernova magnitude measurement uncertainty $\sigma_{\rm mag}$ and a range of uncertainties σ_{Ω_m} in the independent prior knowledge of Ω_m. (As in Fig. 4, the Supergravity model is used here as the example, but the other models give comparable results.) The systematic uncertainties are 0.01 in w_0 and 0.10 in w_1.

in Table 1 and Figure 7), we consider different possible states of prior information about the value of Ω_m, ranging from relatively poorly known ($\sigma_{\Omega_m} \approx 0.15$), roughly the case today, to well determined ($\sigma_{\Omega_m} \approx 0.04$), a possible goal within the next decade. The systematic errors lead to roughly the same contribution as the statistical errors for the case of a perfectly constrained $\sigma_{\Omega_m} = 0.0$. We conclude from Fig. 7 and Table 1 that expanding the fitting function to include w_1 will become useful when the value of Ω_m is better constrained than it is today, as would be the case with complementary measurements from other cosmological probes.

It may be possible to reduce the statistical uncertainties even further, by increasing the sample size and/or by improving the intrinsic luminosity calibration for each supernova. Figure 7 also shows the smaller likelihood region (dotted ellipse) which one gets when taking $\sigma_{\rm mag} = 0.09$ and doubling the number of supernovae in each bin. This means (see Table 1) that the 1σ statistical error on w_1 improves from $\sigma_{w_1} = 0.6$ for the current constraints on Ω_m (solid line in Fig.4), to $\sigma_{w_1} = 0.2$ for future Ω_m constraints (dashed line), to very tight constraints of $\sigma_{w_1} = 0.12$ for the "improved" scenario, with twice as many more-tightly-calibrated supernovae (dotted line).

A Non-parametric Reconstruction

The most general approach to probing the dark energy dynamics is direct reconstruction of $w(z)$ from the measured luminosity distance – redshift relation of SNe Ia data [7, 12, 13]. This method is non-parametric and requires no assumptions about the dark energy or its equation of state. It is also the most challenging approach, since the reconstructed potential and equation of state factor will depend on first and second derivatives of the distance with respect to redshift. This leads to a fundamental problem: even very accurate and dense measurements of $r(z)$ allow great freedom in $r' \equiv dr/dz$ and $r'' \equiv d^2r/dz^2$, because they themselves are not probed directly. To address this problem, various authors have advocated polynomials and Padé approximants [13] and various fitting functions [6, 12] to represent $r(z)$ and thereby reduce the inherent freedom in r' and r''.

In Fig. 8 we show the simulated reconstruction of the quintessence model with potential $V(\phi) = M^4[\exp(m_{PL}/\phi) -$

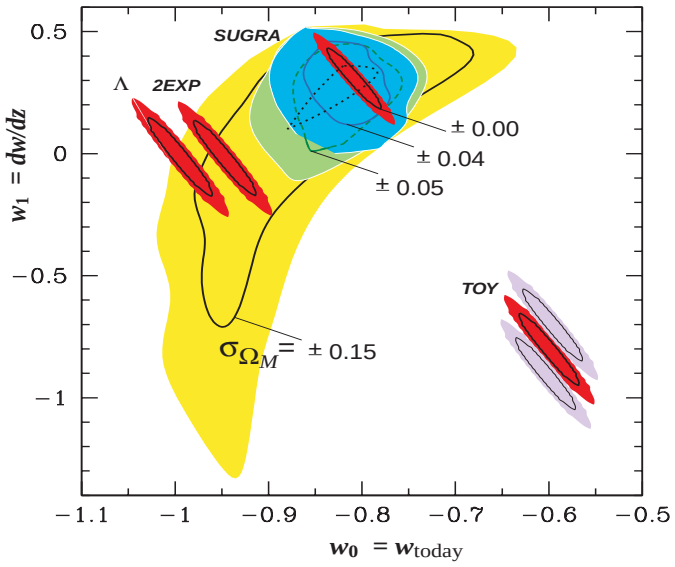

FIG. 7: Separation of dark energy models (labeled as in Fig. 5) in the w_0–w_1 plane. The contours and shaded regions represent the same probabilities as in Fig. 6. For the Supergravity (*SUGRA*) model, a range of increasingly larger contours represents the results using prior knowledge on Ω_m with increasingly poorer uncertainty, σ_{Ω_m}. The black dotted curve corresponds to the projected-1σ error contour obtained for more optimistic dataset specifications ($\sigma_{\rm mag} = 0.09$; see text) with a prior of $0.25 \le \Omega_m \le 0.35$. For the example of the *TOY* model, flanking contours show the effects of a drifting systematic error (see text). The plot is taken from [6].

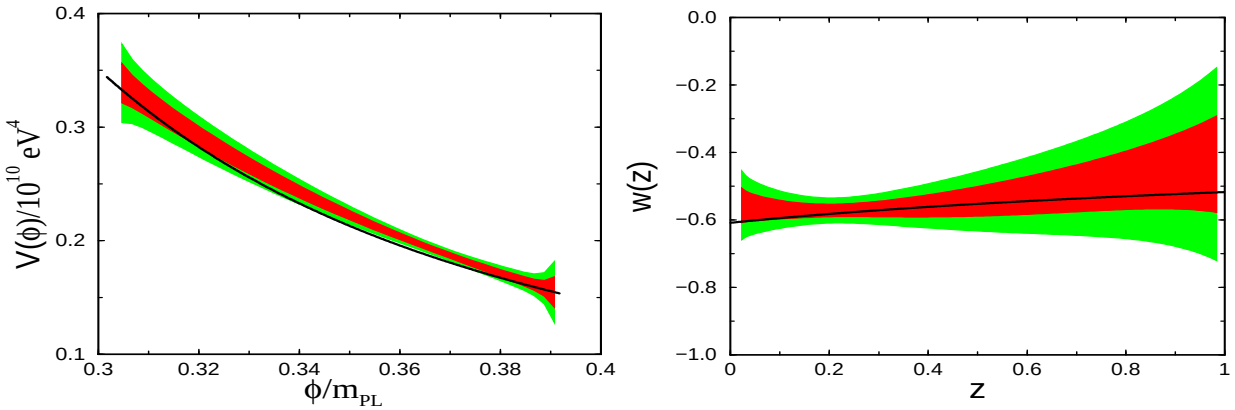

FIG. 8: Reconstruction of the quintessence model with potential $V(\phi) = M^4[\exp(m_{PL}/\phi) - 1]$ [3] and $\Omega_\phi = 0.50$. The solid line is the input model, and the shaded regions show the 68% and 95% confidence, produced from Monte Carlo simulation of 2000 SNe uniformly distributed out to $z = 1.5$ with individual uncertainties of 0.15 mag (7% in distance). A three-parameter Padé approximant fit to $r(z)$ was used. The right panel shows the reconstruction of $w(z) = (\frac{1}{2}\dot\phi^2 - V)/(\frac{1}{2}\dot\phi^2 + V)$. The plot is taken from Ref. [8].

1] [3] and $\Omega_\phi = 0.50$. We assumed 2000 SNe uniformly distributed out to $z = 1.5$ with individual uncertainties of 0.15 mag. Data were fit by a three-parameter Padé approximant of the form

$$H_0\, r(z) = \frac{z(1 + a\, z)}{1 + b\, z + c\, z^2}. \tag{6}$$

We have also tried other suggested fitting functions [6, 12], as well as a piecewise cubic spline with variable tension. All are able to fit the predicted form for $r(z)$ well (about 0.2% accuracy). However, a good fit is not the whole story – $r'(z)$ and $r''(z)$ are equally important – and the small bumps and wiggles between the fit and the actual relation given by the dark energy model are important because they lead to reconstruction error.

In sum, non-parametric reconstruction is very challenging, and an oxymoron: as a practical matter the data must be fit by a smooth function. Nevertheless, in the absence of well motivated dark-energy models, reconstruction offers a more general means of getting at the time dependence of w and the fundamental nature of the dark energy. Finally, obviously the best way to test a specific model is to use *it* as a representation of the dark energy.

IV. CONCLUSIONS

Determining the nature of the dark energy that accounts for 2/3rds of the matter and energy in the Universe and is causing its expansion to accelerate ranks as one of the most important problems in both physics and astronomy. At the moment, there is very little theoretical guidance, and additional experimental constraints are urgently needed.

The first step is to determine the equation of state of the dark energy. Since many proposed dark energy models predict a time-varying equation of state, in contrast to the cosmological constant, measuring its time variation (e.g. dw/dz) is a very important, but difficult task. Alternatively, one can rule out proposed dark energy models by considering the curves they trace out in the Hubble diagram. Finally, the non-parametric reconstruction of either $w(z)$ or the potential energy curve for a quintessence model is the most demanding test, as it requires the first and second derivatives of the coordinate distance $r(z)$.

From our analysis it is clear that a dataset of the sort proposed with SNAP presents an exciting and unique opportunity to constrain theories of cosmic acceleration and fundamental physics.

REFERENCES

[1] M. S. Turner and M. White, Phys. Rev. D, **56**, R4439 (1997)

[2] J. Frieman et al., *Phys. Rev. Lett.* **75**, 2077 (1995), K. Coble, S. Dodelson and J. A. Frieman, *Phys. Rev.* **D55**, 1851 (1997), R. R. Caldwell, R. Dave' and P. J. Steinhardt, *Phys. Rev. Lett.* **80**, 1582 (1998), K. Choi, *Phys. Rev.* **D62**, 043509 (2000), S. Dodelson, M. Kaplinghat and E. Stewart, *Phys. Rev. Lett.* **85**, 5276 (2000).

[3] I. Zlatev, L. Wang and P. J. Steinhardt, *Phys. Rev. Lett.* **82**, 896 (1999)

[4] P. J. Steinhardt, L. Wang and I. Zlatev, *Phys. Rev.* **D 59**, 123504 (1999), Ph. Brax and J. Martin, *Phys. Lett.* **B 468**, 40 (1999), P. Binétruy, *Phys. Rev.* **D60**, 063502 (1999).

[5] A. Cooray and D. Huterer, *Ap. J.* **513**, L95 (1999)

[6] J. Weller and A. Albrecht, *Phys. Rev. Lett.* **86**, 6 (2001)

[7] J. Weller and A. Albrecht, astro-ph/0106079

[8] D. Huterer and M. S. Turner, PRD in press, astro-ph/0012510

[9] B. Ratra and P. J. E. Peebles, *Phys. Rev.* **D37**, 3406 (1988), C. Wetterich, *Astron. Ap.* **301**, 321 (1995), P. G. Ferreira and M. Joyce, *Phys. Rev. Lett.* **79**, 4740 (1997), P. G. Ferreira and M. Joyce, *Phys. Rev.* **D58**, 023503 (1998), E. J. Copeland, A. R. Liddle and D. Wands, *Phys. Rev.* **D57**, 4686 (1998).

[10] A. Albrecht and C. Skordis, *Phys. Rev. Lett.* **84**, 2076 (2000), T. Barreiro, E. J. Copeland and N. J. Nunes, *Phys. Rev.* **D61**, 127301 (2000), J. Weller, astro-ph/0004096.

[11] J. P. Uzan, *Phys. Rev.* **D59**, 123510 (1999), T. Chiba, *Phys. Rev.* **D60**, 083508 (1999), R. Bean and J. Magueijo, astro-ph/0007199, L. Amendola, *Phys. Rev.* **D62**, 043511 (2000), L. Amendola and D. Tocchini-Valentini, astro-ph/0011243.

[12] T. D. Saini et al, *Phys. Rev. Lett.* **85**, 1162 (2000) T. Chiba and T. Nakamura, *Phys. Rev.* **D62**, 121301 (2000)

[13] D. Huterer and M. S. Turner, Phys. Rev. D **60**, 081301 (1999)